RIS-Empowered Ambient Backscatter Communication Systems

D. Loku Galappaththige, *Member, IEEE*, F. Rezaei, *Member, IEEE*, C. Tellambura, *Fellow, IEEE,* Sanjeewa Herath, *Member, IEEE*

***Abstract*—Passive tags must harvest sufficient energy to operate. However, ensuring the tag's energy needs and simultaneously suppressing the interference in ambient backscatter systems is challenging. To meet this, we employ a reconfigurable intelligent surface (RIS) to amplify the ambient source signal that reaches the tag. We maximize the achievable rate by optimizing the RIS phase-shifts subject to the tag's energy harvesting constraint. Specifically, the phase-shifts are optimized to increase the tag's received power while suppressing the direct-and-RIS-cascaded link interference. The optimization problem is non-convex, and we convexify it by means of fractional programming and a quadratic transformation. In comparison to a benchmark, our optimal phase-shift design provides $\sim 150\%$ and $\sim 250\%$ gains in harvested power and achieved rate, respectively, at $20\,\mathrm{dBm}$ transmit power.**

***Index Terms*—Ambient backscatter communication (AmBC), Reconfigurable intelligent surface (RIS), Passive tag.**

I. Introduction

Ambient Backscatter communication (AmBC) is an emerging enabler of passive Internet-of-Things (IoT) networks. Passive backscatter tags reflect external ambient radio frequency (RF) signals to communicate and are powered by energy harvesting (EH). Therefore, such tags have no batteries and eschew power-hungry and costly RF circuits [1]. They are thus low-cost devices with minimal processing capabilities and strict energy constraints. Ambient sources include TV towers, Wi-Fi access points, and cellular base stations (BSs) [1], [2]. AmBC ensures spectrum and energy efficiency and avoids new spectrum allocations.

The main problem with passive tags is the potential lack of energy and attendant problems. The tag typically needs at least $-20\,\mathrm{dBm}$ to activate its circuits. Ambient sources risk a tag-energy outage because of their inherent unpredictability, low power density in the order of $1{\sim}100\,\mu\mathrm{W/cm^2}$, and distance. However, reconfigurable intelligent surfaces (RISs) control the propagation environment advantageously [3]. Hence, deploying a RIS and configuring the phase shifts its elements can enhance the EH potential of the tag, increase the desired signal at the reader, and suppress interference at the reader [4], [5]. However, the RIS can be placed in the forward link (i.e., the RF source-to-tag link) or the tag-to-reader link. The first option delivers more energy to the tag, resulting in improved harvested energy, higher achievable rates, and longer communication ranges with no modifications or additional processing at the tag. This letter investigates that option.

D. Loku Galappaththige, F. Rezaei, and C. Tellambura with the Department of Electrical and Computer Engineering, University of Alberta, Edmonton, AB, T6G 1H9, Canada (e-mail: diluka.lg,rezaeidi,ct4@ualberta.ca).

S. Herath is with the Huawei Canada, 303 Terry Fox Drive, Suite 400, Ottawa, Ontario K2K 3J1 (e-mail: sanjeewa.herath@huawei.com).

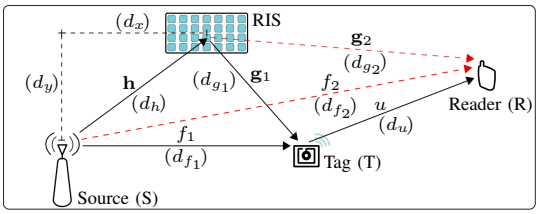

Fig. 1: An RIS-assisted AmBC system setup. Red lines denote interference links. Here, $d_h = \sqrt{d_x^2 + d_y^2}$, $d_{g_1} = \sqrt{(d_{f_1} - d_x)^2 + d_y^2}$, $d_{g_2} = \sqrt{(d_{f_1} + d_u - d_x)^2 + d_y^2}$, and $d_{f_2} = d_{f_1} + d_u$.

***Motivation and Our Contributions**:* The primary aim is to increase the tag activation distance and received power (Fig. 1). A RIS in the source-to-tag link achieves those goals. However, the reflected signal via RIS must be lower than the tag's backscatter signal. Otherwise, the decoding performance of the reader degrades (Remark 1). Hence, the detrimental effects of this interference must be eliminated.

Therefore, we aim to enhance the tag data rate (Fig. 1) by maximizing the received signal-to-interference- plus-noise ratio (SINR) at the reader. This improves the reader's desired signal power and suppresses the interference from the **S**-**R** and **S**-RIS-**R** links. We thus optimize the RIS phase shifts to maximize the tag rate subject to the tag's EH constraint. The optimization problem is not convex, so we convert it into a convex one and solve it using fractional programming. We show that the optimal RIS phase-shift design increases the tag's received power and suppresses the interference from the direct and the cascaded links, achieving significant gains in RIS-empowered AmBC.

A. Previous Contributions on RIS-Assisted AmBC

RIS improves performance of backscatter communication (BackCom) [6], particularly the detection performance and the bit error rate of AmBC [4], [5], [7]–[9]. These works show reliable communications at a moderate signal-to-noise ratio (SNR). Moreover, a RIS can improve the energy efficiency of an AmBC-enabled non-orthogonal multiple access (NOMA) network by assisting cell-edge users [10].

This paper differs from [4], [5], [7]–[9]. Our focus is to maximize the tag rate under EH constraint by optimizing the RIS phase shifts to enhance the desired signal power and suppress the interference terms.

Notation: $\mathbf{A}^{\mathrm{T}}$ and $\mathbf{A}^{\mathrm{H}}$, denote transpose and Hermitian transpose, respectively. $\mathbb{E}\{\cdot\}$ denotes the statistical expectation. Finally, $\mathcal{CN}(\boldsymbol{\mu}, \mathbf{C})$ is a complex Gaussian vector with mean $\boldsymbol{\mu}$ and co-variance matrix $\mathbf{C}$.

II. System, Channel, and Signal Models

A. System and Channel Models

We consider a RIS-empowered AmBC network having a single-antenna source (**S**), a single-antenna reader (**R**), a single-antenna tag (**T**), and a RIS consisting of N passive reflectors (Fig. 1). **R** is assumed to be a cooperative receiver that decodes the tag's data only (i.e., no primary data) [11]. Hence, the primary purpose of the RIS used in the **S**-**T** link is to supply as much power to the passive tag as possible. In particular, we optimize the RIS phase shifts to maximize the tag's received power and the reader's received SINR. The RIS control unit can run the algorithm we develop to achieve this task. We take the symbiotic viewpoint that the ambient source will help to improve the performance of the AmBC network. To this end, we assume a backhaul connection between the RIS and the RF source [3]. We label the set of passive RIS reflectors as $\mathcal{N} = \{1, \ldots, N\}$.

The direct channels, **S**-**T**, **S**-**R**, and **T**-**R** are denoted as f_1, f_2, and u, respectively. Moreover, the reflective channels, **S**-RIS, RIS-**T**, and RIS-**R** are denoted as $\mathbf{h} = [h_1, \ldots, h_N]^{\mathrm{T}} \in \mathbb{C}^{N\times 1}$, $\mathbf{g}_k = [g_{k,1}, \ldots, g_{k,N}]^{\mathrm{T}} \in \mathbb{C}^{N\times 1}$, $k \in \{1, 2\}$, respectively. A unified representation of all channels is given as

$$a = \alpha_a \exp(j\phi_a), \tag{1}$$

where $a \in \mathcal{A} = \{f_1, f_2, u, h_n, g_{1,n}, g_{2,n}\}, n \in \mathcal{N}$ and $\phi_a \in [-\pi, \pi]$ is the phase of a. In (1), α_a is the envelope of a, which is assumed to be Nakagami-m distributed with m_a shape and $\Omega_a = m_a\zeta_a$ scaling parameters. Here, ζ_a accounts for the large-scale path loss and shadowing. Since the RIS elements are co-located, the large-scale parameters are identical, i.e., $\zeta_{g_{k,n}} = \zeta_{g_k},\ k \in \{1, 2\}$, and $\zeta_{h_n} = \zeta_h$ for $n \in \mathcal{N}$. We assume the availability of channel state information (CSI). Although CSI estimation is complicated in AmBC systems, some results are emerging (see [12] and reference therein).

B. EH at the Passive Tag

Passive tags perform EH and data transmission simultaneously via the power-splitting mode [13]. Each task takes a fraction of the incident RF power on the tag.

Let P_T be the received power at **T**, and it backscatters αP_T of the received RF power and absorbs $(1-\alpha)P_T$ for EH, where $\alpha \in (0, 1)$ is the reflection coefficient of the tag[1]. Here, we adopt the linear EH model, and the harvested power at the tag is given as

$$P_h = \beta(1-\alpha)P_T, \tag{2}$$

where β, $(0 \le \beta < 1)$, is the power conversion efficiency, e.g., typical values of $\beta = \{0.2, 0.4, 0.6\}$ [14]. Although practical EH circuits exhibit non-linear operating characteristics and an activation threshold, the linear model can be accurate for certain operating regions. However, non-linear EH models are widely used as well (see [15], [16] and references therein). Our solution can be extended to such models as well. We omit the details for brevity.

[1]To keep α constant, we use constant envelope modulation (M-ary phase shift keying).

C. Signal Model

S transmits a modulated carrier signal $\sqrt{P}s$, where P is the transmit power and signal s satisfies $\mathbb{E}\{|s|^2\} = 1$. **T** receives it through the direct channel, f_1, and the reflective channels of the RIS, $\mathbf{g}_1$. The received signal at **T** is given as

$$y_T = \sqrt{P}(f_1 + \mathbf{g}_1^{\mathrm{T}}\boldsymbol{\Theta}\mathbf{h})s, \tag{3}$$

where $\boldsymbol{\Theta} = \mathrm{diag}\,(\theta_1, \ldots, \theta_N) \in \mathbb{C}^{N\times N}$ is a diagonal matrix which captures the reflection properties (the magnitude of attenuation and the phase-shift) of the RIS elements. Moreover, $\theta_n = \eta_n e^{j\phi_n}$, $n \in \mathcal{N}$, is the complex-valued reflection coefficient at the n-th reflector, where η_n is the magnitude of attenuation and $\phi_n \in [-\pi, \pi]$ is the n-th reflector phase-shift.

According to Section II-B, **T** must harvest enough power to support its internal operations. Therefore, with the linear EH model (2), the received power at **T** must satisfy the following energy constraint:

$$\beta(1-\alpha)P_T \ge P_b, \tag{4}$$

where $P_T = P|f_1 + \mathbf{g}_1^{\mathrm{T}}\boldsymbol{\Theta}\mathbf{h}|^2$ is the received power at **T** and P_b is the activation threshold of energy harvester at **T**.

T harvests energy from the received signal and modulates it with its data, q, where q is the normalized backscatter symbol selected from a multi-level (M-ary) modulation such that $\mathbb{E}\{|q|^2\} = 1$, before transmitting it to **R**. The received signal at **R** is given as

$$y_R = \sqrt{\alpha P}u(f_1 + \mathbf{g}_1^{\mathrm{T}}\boldsymbol{\Theta}\mathbf{h})sq + \sqrt{P}(f_2 + \mathbf{g}_2^{\mathrm{T}}\boldsymbol{\Theta}\mathbf{h})s + z, \tag{5}$$

where $z \sim \mathcal{CN}(0, \sigma_z^2)$ is the additive white Gaussian noise (AWGN) at **R** with mean 0 and variance σ_z^2. The data detection task of **R** is to estimate the value of q. The second term on the right-hand side is the cumulative direct interference and the RIS reflected interference (red dash-lines in Fig. 1). Ideally, this term must be eliminated by the SIC circuit [11]. However, perfect SIC may not always be feasible, and a decoding error may occur during the SIC process. Hence, using (5), the received signal to decode the tag's signal after the imperfect SIC process can be written as

$$\begin{aligned}\bar{y}_R &= y_R - \sqrt{P}(f_2 + \mathbf{g}_2^{\mathrm{T}}\boldsymbol{\Theta}\mathbf{h})\hat{s},\\ &= \sqrt{\alpha P}u(f_1 + \mathbf{g}_1^{\mathrm{T}}\boldsymbol{\Theta}\mathbf{h})sq + \sqrt{P}(f_2 + \mathbf{g}_2^{\mathrm{T}}\boldsymbol{\Theta}\mathbf{h})(s - \hat{s}) + z,\end{aligned} \tag{6}$$

where $\hat{s}$ is the decoded signal (the estimate of s)[2].

Therefore, using (6), the received SINR at **R** may be expressed as

$$\gamma = \frac{\alpha P|u(f_1 + \mathbf{g}_1^{\mathrm{T}}\boldsymbol{\Theta}\mathbf{h})|^2}{2(1-\rho)P|(f_2 + \mathbf{g}_2^{\mathrm{T}}\boldsymbol{\Theta}\mathbf{h})|^2 + \sigma_z^2}, \tag{7}$$

where $\rho \in [0, 1]$ determines the degree of imperfectness of the SIC operation [17]. Next, the achievable rate at **R** is

$$\mathcal{R} = \log_2(1 + \gamma)\ \text{bps/Hz}. \tag{8}$$

[2]Without loss of generality, s and its estimate $\hat{s}$ can be assumed as jointly Gaussian with a certain correlation coefficient [17], i.e., $s = \rho\hat{s} + e$, where $\hat{s} \sim \mathcal{CN}(0, 1)$ and $e \sim \mathcal{CN}(0, \sigma_e^2/[1 + \sigma_e^2])$ is the estimation error and is statistically independent of $\hat{s}$.

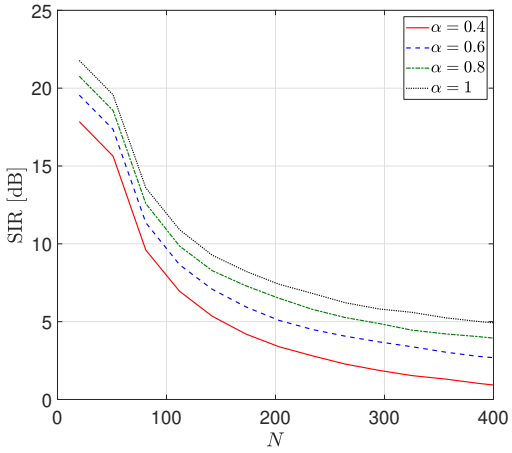

Fig. 2: The SIR for $d_y = 1\,\text{m}$, $d_x = 8\,\text{m}$, $d_{f_1} = 10\,\text{m}$, and $d_u = 10\,\text{m}$.

Remark 1. *To highlight the detrimental effects of interference from the direct link and the cascaded RIS channel, we investigate the signal-to-interference ratio (SIR) at* $\mathbf{R}$*, which can be expressed as*

$$SIR = \frac{\alpha |u\left(f_1 + \mathbf{g}_1^{\mathrm{T}} \boldsymbol{\Theta}^{\star} \mathbf{h}_1\right)|^2}{|f_2 + \mathbf{g}_2^{\mathrm{T}} \boldsymbol{\Theta}^{\star} \mathbf{h}|^2}, \tag{9}$$

where $\boldsymbol{\Theta}^{\star}$ *is the optimal phase-shift matrix obtained by maximizing the desired signal component. From (3), we can determine how to maximize* $\mathbf{T}$*'s received signal power, which also increases desired power at* $\mathbf{R}$*. Thus, the RIS phases should be chosen to maximize* $|f_1 + \mathbf{g}_1^{\mathrm{T}} \boldsymbol{\Theta}^{\star} \mathbf{h}_1|$*. This happens when all the terms add constructively to* f_1*, i.e.,* $\phi_f = \phi_{g_n} + \phi_{h_n} + \phi_n$*, where* $\phi_a \in [-\pi, \pi]$ *is the phase of* $a \in \mathcal{A}$*. Therefore, the* n*-th RIS phase-shift is adjusted as* $\phi_n^{\star} = \max_{-\pi \le \phi_n \le \pi} P_T = \phi_f - (\phi_{g_n} + \phi_{h_n}),\ n \in \mathcal{N}$ *[18].*

In Fig. 2, the SIR (9) *is plotted for different numbers of RIS elements. Notice the unexpected trend of SIR decreasing with increasing* N*. Since* $\boldsymbol{\Theta}^{\star}$ *is designed without considering interference, constructive additions of interference can occur at* $\mathbf{R}$ *(this probability grows with* N*). We can see that even for a vast number of RIS elements, the SIR is* $\sim 2\,\text{dB}$*, i.e., there is not much difference between desired signal power and the interference power. Hence, the latter cannot simply be neglected compared to the former. Moreover, the choice of* $\boldsymbol{\Theta}^{\star}$ *is not optimal overall. The solution is to employ some degrees of freedom RIS offers to suppress this interference. With this goal in mind, we next develop an optimization framework to maximize the achievable rate while minimizing this interference.*

III. Problem Formulation and Proposed Solution

A. Problem Formulation

We aim to optimize the RIS phase-shifts to maximize both the received signal power at $\mathbf{T}$ and the achievable rate/SINR at $\mathbf{R}$. Thus, an optimization problem is formulated as follows:

$$\mathcal{P}_1 : \underset{\boldsymbol{\Theta}}{\text{maximize}} \ \log_2(1+\gamma), \tag{10a}$$

$$\text{subject to} \ \beta(1-\alpha)P|f_1 + \mathbf{g}_1^{\mathrm{T}} \boldsymbol{\Theta} \mathbf{h}|^2 \ge P_b, \tag{10b}$$

$$|\theta_n| \le 1. \tag{10c}$$

Here, the constraint (10b) guarantees the minimum operating energy requirement for $\mathbf{T}$. Due to the non-convex objective function and the constraint, the problem $\mathcal{P}_1$ cannot be solved by using conventional convex optimization methods. Therefore, we next convexify these non-convex objective and the constraint to solve the optimization problem, $\mathcal{P}_1$.

B. Proposed Solution

First, we define $\mathbf{a}_1 \triangleq \text{diag}(\text{u}\mathbf{g}_1^{\mathrm{T}})\mathbf{h}$ and $\mathbf{a}_2 \triangleq \text{diag}(\mathbf{g}_2^{\mathrm{T}})\mathbf{h}$. Thereby, the SINR in (7) is rearranged as

$$\gamma = \frac{\alpha P |b_1 + \boldsymbol{\theta}^{\mathrm{H}} \mathbf{a}_1|^2}{2(1-\rho)P|b_2 + \boldsymbol{\theta}^{\mathrm{H}} \mathbf{a}_2|^2 + \sigma_z^2}, \tag{11}$$

where $b_1 \triangleq u f_1$, $b_2 \triangleq f_2$, and $\boldsymbol{\theta} = [\theta_1, \ldots, \theta_N]^{\mathrm{T}}$. Then, $\mathcal{P}_1$ can be treated as a fractional programming problem [19]. We next apply a quadratic transform to the objective function of $\mathcal{P}_1$ as

$$f(\boldsymbol{\theta}, \lambda) = \log_2\Big(1 + 2\lambda\sqrt{\alpha \mathrm{P}}\text{Re}\left\{\mathrm{b}_1 + \boldsymbol{\theta}^{\mathrm{H}} \mathbf{a}_1\right\} - \lambda^2\left(2(1-\rho)P|b_2 + \boldsymbol{\theta}^{\mathrm{H}} \mathbf{a}_2|^2 + \sigma_z^2\right)\Big), \tag{12}$$

where λ is an auxiliary variable introduced by the quadratic transformation. Thereby, we alternatively optimize $\boldsymbol{\theta}$ and λ. For a given $\boldsymbol{\theta}$, the optimal λ is found in closed-form as [19]

$$\lambda^o = \frac{\alpha\sqrt{P}\text{Re}\left\{\mathrm{b}_1 + \boldsymbol{\theta}^{\mathrm{H}} \mathbf{a}_1\right\}}{\ln(2)\left(2(1-\rho)P|b_2 + \boldsymbol{\theta}^{\mathrm{H}} \mathbf{a}_2|^2 + \sigma_z^2\right)}. \tag{13}$$

Remark 2. *Without compromising generality, we confine that the phase-shift vector,* $\boldsymbol{\theta}$*, with the channel responses to produce a non-negative real desired signal term, i.e.,* $\left|b_1 + \boldsymbol{\theta}^{\mathrm{H}} \mathbf{a}_1\right| \approx \text{Re}\{\mathrm{b}_1 + \boldsymbol{\theta}^{\mathrm{H}} \mathbf{a}_1\}$*. Our simulation results also demonstrate the validity of this approach. This is because our approach iteratively maximizes the achievable rate/SINR by co-phasing the desired signal component while reducing interference.*

In this optimization problem, we must optimize $\boldsymbol{\theta}$ for a given λ. First, by expanding $|b_i + \boldsymbol{\theta}\mathbf{a}_i|^2$ and then applying several mathematical manipulations, the objective function in (12) can be rearranged as

$$f(\boldsymbol{\theta}) = \log_2\left(1 - \boldsymbol{\theta}^{\mathrm{H}}\mathbf{U}\boldsymbol{\theta} + 2\text{Re}\left\{\boldsymbol{\theta}^{\mathrm{H}}\mathbf{v}\right\} + \mathrm{c}\right), \tag{14}$$

where $\mathbf{U}$, $\mathbf{v}$, and c are defined as

$$\mathbf{U} \triangleq 2(\lambda^o)^2(1-\rho)P\mathbf{a}_2\mathbf{a}_2^{\mathrm{H}}, \tag{15a}$$

$$\mathbf{v} \triangleq 2\lambda^o\sqrt{\alpha P}\mathbf{a}_1 - 2(\lambda^o)^2(1-\rho)Pb_2^*\mathbf{a}_2, \tag{15b}$$

$$c \triangleq 2\lambda^o\sqrt{\alpha P}\text{Re}\{\mathrm{b}_1\} - (\lambda^{\mathrm{o}})^2\left(2(1-\rho)\mathrm{P}|\mathrm{b}_2|^2 + \sigma_{\mathrm{z}}^2\right). \tag{15c}$$

Next, the corresponding optimization problem can be given as

$$\mathcal{P}_2 : \underset{\boldsymbol{\theta}}{\text{maximize}} \ f(\boldsymbol{\theta}), \tag{16a}$$

$$\text{subject to} \ \beta(1-\alpha)P_{\mathrm{T}}^{\mathrm{Lin}} \ge P_b, \tag{16b}$$

$$|\theta_n| \le 1, \tag{16c}$$

where $P_{\mathrm{T}}^{\mathrm{Lin}}$ is the linearized received signal power at $\mathbf{T}$, given as (Appendix A)

$$P_{\mathrm{T}}^{\mathrm{Lin}} = \boldsymbol{\theta}_{i-1}^{\mathrm{H}}\mathbf{U}_0\boldsymbol{\theta}_{i-1} + 2\text{Re}\left\{\boldsymbol{\theta}_{\mathrm{i-1}}^{\mathrm{H}}\mathbf{v}_0\right\} + \mathrm{c}_0 + \left(\left(\mathbf{U}_0 + \mathbf{U}_0^{\mathrm{H}}\right)\boldsymbol{\theta}_{i-1} + 2\text{Re}\left\{\mathbf{v}_0\right\}\right)^{\mathrm{H}}\left(\boldsymbol{\theta}_i - \boldsymbol{\theta}_{i-1}\right), \tag{17}$$

where $\mathbf{a}_0 \triangleq \text{diag}(\mathbf{g}_1^{\text{T}})\mathbf{h}$, $b_0 \triangleq f_1$, $\mathbf{U}_0 \triangleq P\mathbf{a}_0\mathbf{a}_0^{\text{H}}$, $\mathbf{v}_0 \triangleq Pb_0^*\mathbf{a}_0$, and $c_0 \triangleq P|b_0|^2$. Besides, $\boldsymbol{\theta}_i$ and $\boldsymbol{\theta}_{i-1}$ are the current and the previous iteration values of $\boldsymbol{\theta}$.

Because $\mathbf{a}_2\mathbf{a}_2^{\text{H}}$ is a positive-definite matrix, $\mathbf{U}$ is also a positive-definite matrix. Hence, the objective function, $f(\boldsymbol{\theta})$, is a quadratic concave function of $\boldsymbol{\theta}$. Consequently, $\mathcal{P}_2$ can be solved as a quadratically constrained quadratic program (QCQP) [20]. Algorithm 1 gives the solution of $\mathcal{P}_2$.

Algorithm 1 : Algorithm for phase-shift optimization.

Initialization: Initialize $\boldsymbol{\theta}$ to a feasible value.
Repeat
Step 1: Update λ by (13).
Step 2: Update $\boldsymbol{\theta}$ by solving $\mathcal{P}_2$ in (16).
Until the value of the objective function converges.
Output: The optimal phase-shift matrix $\boldsymbol{\Theta}^o$.

Remark 3. *The Algorithm 1 presents the proposed optimization technique for solving $\boldsymbol{\Theta}$ once the original problem, $\mathcal{P}_1$, is converted into a convex problem. $\mathcal{P}_1$ is iteratively solved using an alternating optimization technique. First, we quantify the SINR in* (11) *upon initializing $\boldsymbol{\Theta}$, and then we update a better solution for $\boldsymbol{\Theta}$ in each iteration. This procedure is repeated until the normalized objective function increases less than $\epsilon = 10^{-4}$.*

Remark 4. *Since the tag is a passive device with limited power, $\mathcal{P}_1$ considers a fixed α to maintain the minimum power, low cost, and small form factor of the tag [21]. However, α can also be optimized at the expense of a simple tag design. Since $\boldsymbol{\Theta}$ and α are independent variables, we can readily use alternative optimization. Thereby, $\boldsymbol{\Theta}$ and α are alternatively optimized until the convergence. We omit the details for brevity.*

IV. Simulation Results

This section presents simulation results to evaluate the system performance. We adopt the 3GPP UMi model to model the large-scale fading ζ_a with $f_c = 3\,\text{GHz}$ operating frequency [22, Table B.1.2.1]. Moreover, AWGN variance is modeled as $\sigma_z^2 = 10\log_{10}(N_0 B N_f)$ dBm, where $N_0 = -174\,\text{dBm/Hz}$, $B = 10\,\text{MHz}$ is the bandwidth, and $N_f = 10\,\text{dB}$ is the noise figure. Additionally, the activation threshold of the tag, P_b, is set to $-20\,\text{dBm}$ and unless otherwise specified, the Nakagami-m parameter, m_a, is set to 1.

We consider four different scenarios of $\boldsymbol{\Theta}$ including three benchmarks and the proposed scheme:

- C_1 *Random*: $\boldsymbol{\Theta}$ is randomly designed.
- C_2 *Ideal - Desired power enhancement with perfect SIC assumption*: i.e., **R** cancels interference from both direct and RIS cascaded links perfectly. In this case, the optimal choice of phases is given by $\boldsymbol{\Theta}^\star$ found in Remark 1, where the desired received power at **T** is maximized. This ideal case yields a valuable upper bound for performance evaluations.
- C_3 *Imperfect SIC - Omitting the interference but considering imperfect SIC*: $\boldsymbol{\Theta}^\star$ is designed, as per Remark 1, to maximize the received power at **T**. However, the performances depend on the precision of the SIC operation (i.e., $\rho < 1$).
- C_4 *Optimal (Proposed) - Desired power enhancement while suppressing the interference*: $\boldsymbol{\Theta}$ is found through the optimization problem (10) and Algorithm 1.

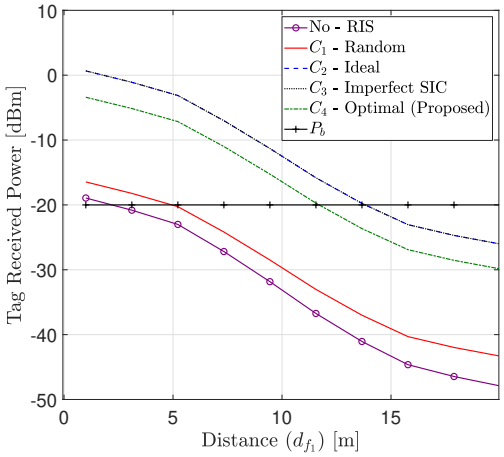

Fig. 3: The average achievable rate versus distance for $P = 20\,\text{dBm}$, $N = 100$, $d_y = 1\,\text{m}$, $d_x = 1\,\text{m}$, $d_u = 10\,\text{m}$, $\beta = 0.6$, $\alpha = 0.6$, and $\rho = 0.95$.

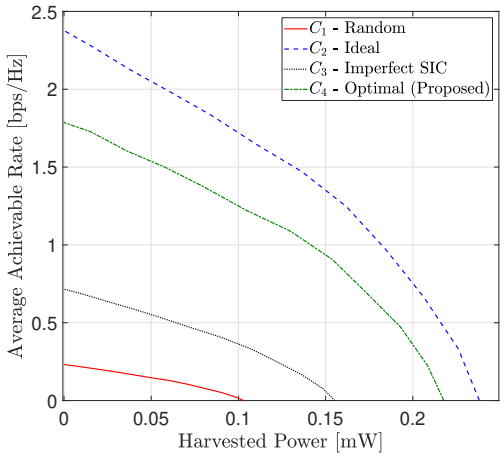

Fig. 4: The trade-off between the harvested power and the achievable rate for $P = 20\,\text{dBm}$, $N = 100$, $d_x = 8\,\text{m}$, $d_y = 1\,\text{m}$, $d_{f_1} = 10\,\text{m}$, $d_u = 10\,\text{m}$, $\beta = 0.6$, $\alpha = 0.6$, and $\rho = 0.95$.

Fig. 3 investigates **T**'s activation range under the four scenarios. The received signal power at **T** is plotted as a function of **S**-**T** distance, d_{f_1}. Note that the RIS in the power-up link allows **T** to be activated farther away from **S** than otherwise. Our algorithm increases this range compared to random phase shifts. Since C_2 and C_3 cases optimize $\boldsymbol{\Theta}$ only considering **S**-IRS-**T** channels, both can deliver more power to **T**, resulting high activation range. Despite having slightly less range than C_2 and C_3, C_4 increases the tag activation distance compared to the no-RIS case and C_1.

Fig. 4 depicts the trade-off between the harvested energy and the achieved rate as a function of the α at **T** with different RIS phase-shift designs for transmitting power $P = 20\,\text{dBm}$. As α approaches 1, **T** reflects most of the received power and achieves the maximum rate. However, this operating point is infeasible for a passive tag. In contrast, when α approaches 0, **T** harvests most of the received power, and the achieved rate becomes infinitesimal. Hence, for given α, the rate and harvested power at **T** can be obtained by traversing the trade-

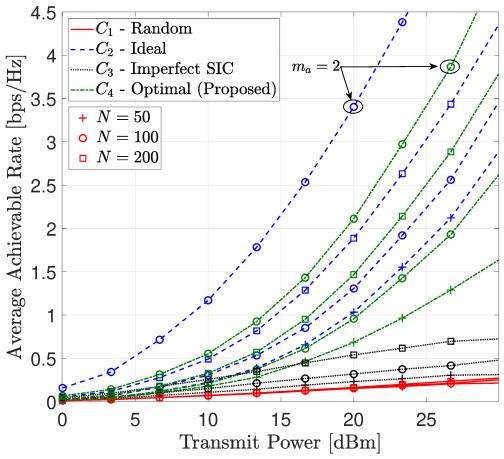

Fig. 5: The achievable rate versus transmit power for $N = \{50, 100, 200\}$, $d_x = 8\,\text{m}$, $d_y = 1\,\text{m}$, $d_{f_1} = 10\,\text{m}$, $d_u = 10\,\text{m}$, $\beta = 0.6$, $\alpha = 0.6$, and $\rho = 0.95$.

off curve. Because $\mathbf{T}$ is passive, it must harvest a minimum power to operate hence $\alpha \in (0, 1)$. Fig. 4 shows that C_4 ensures that $\mathbf{T}$ receives more power to be harvested while suppressing the interference, and hence $\mathbf{T}$ achieves a higher rate as well, compared to C_1 and C_3. C_2 represents the ideal performance. However, proposed C_4 achieves significant gains compared to C_1 and C_3.

Fig. 5 shows the average achieved rate of $\mathbf{T}$ against the transmit power at $\mathbf{S}$ for different numbers of RIS elements N. The proposed optimal RIS phase-shift design (C_4) performs close to the upper bound C_2 and achieves significant gains (compared to C_1 and C_3), as it maximized the received power at $\mathbf{T}$ while suppressing the interference from the direct and cascaded links at $\mathbf{R}$. In particular, with $P = 20\,\text{dBm}$, $N = 100$, and $m_a = 1$, the achieved rate through the optimal design with perfect SIC (C_2), and the proposed optimal one (C_4) are respectively $1.35\,\text{bps/Hz}$ and $0.98\,\text{bps/Hz}$. While with the two other Scenarios, random design C_1 and the optimal design where interference is neglected (C_3), the achieved rates are respectively $0.2\,\text{bps/Hz}$ and $0.35\,\text{bps/Hz}$. Moreover, the achievable rate trend scales with the severity of the fading model, i.e., high achievable rates for large m values.

V. Conclusion

This letter investigated the achievable rate improvements in a RIS-empowered AmBC. We designed optimal RIS phase shifts to simultaneously increase the tag's received power and suppress the direct-and cascaded-RIS link interference. We observed that, with optimal phase shifts, the tag could harvest enough power for its operation and achieve effective rates. Using RIS between the tag and the reader also offers significant gains and is a future research direction.

Appendix A
Linearized Received Power $P_{\text{T}}^{\text{Lin}}$

In order to convert the EH constraint in (10b) to convex form, we first define $\mathbf{a}_0 \triangleq \text{diag}(\mathbf{g}_1^{\text{T}})\mathbf{h}$ and $b_0 \triangleq f_1$. Thereby, the received power at $\mathbf{T}$, $P_T = P|f_1 + \mathbf{g}_1^{\text{T}}\boldsymbol{\Theta}\mathbf{h}|^2 = P|b_0 + \boldsymbol{\theta}^{\text{H}}\mathbf{a}_0|^2$, is expanded as follows:

$$P_T = \boldsymbol{\theta}^{\text{H}}\mathbf{U}_0\boldsymbol{\theta} + 2\text{Re}\left\{\boldsymbol{\theta}^{\text{H}}\mathbf{v}_0\right\} + \text{c}_0, \tag{18}$$

where $\mathbf{U}_0 \triangleq P\mathbf{a}_0\mathbf{a}_0^{\text{H}}$, $\mathbf{v}_0 \triangleq Pb_0^*\mathbf{a}_0$, and $c_0 \triangleq P|b_0|^2$. By applying Taylor series linearization techniques, the linearized received power at $\mathbf{T}$ is obtained as (17).

References

[1] D. T. Hoang, D. Niyato, D. I. Kim, N. V. Huynh, and S. Gong, *Ambient Backscatter Communication Networks*. Cambridge University Press, 2020.

[2] F. Rezaei, C. Tellambura, and S. Herath, "Large-scale wireless-powered networks with backscatter communications—A comprehensive survey," *IEEE open j. Commun. Soc.*, vol. 1, pp. 1100–1130, July 2020.

[3] Q. Wu and R. Zhang, "Intelligent reflecting surface enhanced wireless network via joint active and passive beamforming," *IEEE Trans. Wireless Commun.*, vol. 18, pp. 5394–5409, Nov. 2019.

[4] X. Jia and X. Zhou, "IRS-assisted ambient backscatter communications utilizing deep reinforcement learning," *IEEE Wireless Commun. Lett.*, vol. 10, pp. 2374–2378, Nov. 2021.

[5] S. Idrees, X. Jia, S. Durrani, and X. Zhou, "Design of intelligent reflecting surface (IRS)-boosted ambient backscatter systems," *IEEE Access*, vol. 10, pp. 65000–65010, June 2022.

[6] Y.-C. Liang, Q. Zhang, J. Wang, R. Long, H. Zhou, and G. Yang, "Backscatter communication assisted by reconfigurable intelligent surfaces," *Proceedings of the IEEE*, pp. 1–19, Early Access 2022.

[7] M. Nemati, J. Ding, and J. Choi, "Short-range ambient backscatter communication using reconfigurable intelligent surfaces," in *IEEE Wireless Commun. and Netw. Conf. (WCNC)*, pp. 1–6, May 2020.

[8] Y. Chen, "Performance of ambient backscatter systems using reconfigurable intelligent surface," *IEEE Commun. Lett.*, vol. 25, pp. 2536–2539, Aug. 2021.

[9] R. Fara, D.-T. Phan-Huy, P. Ratajczak, A. Ourir, M. Di Renzo, and J. De Rosny, "Reconfigurable intelligent surface-assisted ambient backscatter communications – experimental assessment," in *IEEE Int. Conf. Commun. Workshops (ICC Workshops)*, pp. 1–7, June 2021.

[10] Y. Zhuang, X. Li, H. Ji, and H. Zhang, "Exploiting intelligent reflecting surface for energy efficiency in ambient backscatter communication-enabled NOMA networks," *IEEE Trans. Green Commun. Netw.*, vol. 6, pp. 163–174, Mar. 2022.

[11] R. Long, Y.-C. Liang, H. Guo, G. Yang, and R. Zhang, "Symbiotic radio: A new communication paradigm for passive internet of things," *IEEE Internet Things J.*, vol. 7, no. 2, pp. 1350–1363, 2020.

[12] S. Ma, G. Wang, R. Fan, and C. Tellambura, "Blind channel estimation for ambient backscatter communication systems," *IEEE Commun. Lett.*, vol. 22, no. 6, pp. 1296–1299, 2018.

[13] R. Zhang and C. K. Ho, "MIMO broadcasting for simultaneous wireless information and power transfer," *IEEE Trans. Wireless Commun.*, vol. 12, pp. 1989–2001, May 2013.

[14] X. Xu, A. Özçelikkale, T. McKelvey, and M. Viberg, "Simultaneous information and power transfer under a non-linear RF energy harvesting model," in *IEEE Int. Conf. on Commun. Workshops (ICC Workshops)*, pp. 179–184, 2017.

[15] Y. Ye, L. Shi, X. Chu, G. Lu, and S. Sun, "Mutualistic cooperative ambient backscatter communications under hardware impairments," *IEEE Trans. Commun.*, pp. 1–1, 2022.

[16] D. Wang, F. Rezaei, and C. Tellambura, "Performance analysis and resource allocations for a WPCN with a new nonlinear energy harvester model," *IEEE Open Journal of the Comm. Soc.*, vol. 1, pp. 1403–1424, 2020.

[17] S. M. Kay, *Fundamentals of Statistical Signal Processing: Estimation Theory*. Englewood Cliffs, NJ, USA: Prentice-Hall, 1993.

[18] W. Zhao, G. Wang, S. Atapattu, T. A. Tsiftsis, and X. Ma, "Performance analysis of large intelligent surface aided backscatter communication systems," *IEEE Wireless Commun. Lett.*, vol. 9, pp. 962–966, July 2020.

[19] K. Shen and W. Yu, "Fractional Programming for Communication Systems-Part I: Power Control and Beamforming," *IEEE Trans. Signal Process.*, vol. 66, no. 10, pp. 2616–2630, 2018.

[20] S. Boyd and L. Vandenberghe, *Convex Optimization*. Cambridge University Press, March 2004.

[21] "3GPP TSG RAN −97e3, Study on ambient IoT , 9.1 (from RP-222685)," Sep. 2022. Available Online: https://portal.3gpp.org/ngppapp/TdocList.aspx?meetingId=60043.

[22] "3GPP TR 36.814, further advancements for E-UTRA physical layer aspects, V.9.0.0 Rel. 9," Mar. 2010. Available Online: https://portal.3gpp.org/desktopmodules/Specifications/SpecificationDetails.aspx?specificationId=2493.